

# Optical and near-IR spectroscopy of candidate red galaxies in two $z \sim 2.5$ proto-clusters<sup>★</sup>

M. Doherty<sup>1</sup>, M. Tanaka<sup>2</sup>, C. De Breuck<sup>2</sup>, C. Ly<sup>3</sup>, T. Kodama<sup>4</sup>, J. Kurk<sup>5,6</sup>, N. Seymour<sup>7</sup>, J. Vernet<sup>2</sup>, D. Stern<sup>8</sup>, B. Venemans<sup>2</sup>, M. Kajisawa<sup>4,9</sup>, and I. Tanaka<sup>10</sup>

<sup>1</sup> European Southern Observatory, ESO Santiago, Alonso de Cordova 3107, Vitacura, Santiago; e-mail: mdoherty@eso.org

<sup>2</sup> European Southern Observatory, ESO Garching, Karl-Schwarzschild-Str 2, D-85748, Garching, Germany

<sup>3</sup> Department of Physics and Astronomy, University of California, Los Angeles, Box 951547, CA 90095, USA

<sup>4</sup> National Astronomical Observatory of Japan, Mitaka, Tokyo 181-8588, Japan

<sup>5</sup> Max Planck Institut für Astronomie, Königstuhl 17, D-69117, Heidelberg, Germany

<sup>6</sup> Max Planck Institut für Extraterrestrische Physik, Giessenbachstrasse, D-68165, Garching, Germany

<sup>7</sup> Mullard Space Science Laboratory, UCL, Holmbury St Mary, Dorking, Surrey RH5 6NT, UK

<sup>8</sup> Jet Propulsion Laboratory, California Institute of Technology, 4800 Oak Grove Dr., Pasadena, CA91109, USA

<sup>9</sup> Subaru Telescope, National Astronomical Observatory of Japan, 650 North Aohoku Place, Hilo, HI96720, USA

<sup>10</sup> Astronomical Institute, Tohoku University, Aramaki, Aoba, Sendai 980-8578, Japan

Received July 10, 2009; accepted November 3, 2009

## ABSTRACT

We present a spectroscopic campaign to follow-up red colour-selected candidate massive galaxies in two high redshift proto-clusters surrounding radio galaxies. We observed a total of 57 galaxies in the field of MRC 0943–242 ( $z = 2.93$ ) and 33 in the field of MRC 1138–262 ( $z = 2.16$ ) with a mix of optical and near-infrared multi-object spectroscopy.

We confirm two red galaxies in the field of MRC 1138–262 at the redshift of the radio galaxy. Based on an analysis of their spectral energy distributions, and their derived star formation rates from the H $\alpha$  and 24  $\mu$ m flux, one object belongs to the class of dust-obscured star-forming red galaxies, while the other is evolved with little ongoing star formation. This result represents the first red and mainly passively evolving galaxy to be confirmed as companion galaxies in a  $z > 2$  proto-cluster. Both red galaxies in MRC 1138–262 are massive, of the order of  $4 - 6 \times 10^{11} M_{\odot}$ . They lie along a Colour-Magnitude relation which implies that they formed the bulk of their stellar population around  $z = 4$ .

In the MRC 0943–242 field we find no red galaxies at the redshift of the radio galaxy but we do confirm the effectiveness of our  $JHK_s$  selection of galaxies at  $2.3 < z < 3.1$ , finding that 10 out of 18 (56%) of  $JHK_s$ -selected galaxies whose redshifts could be measured fall within this redshift range. We also serendipitously identify an interesting foreground structure of 6 galaxies at  $z = 2.6$  in the field of MRC 0943–242. This may be a proto-cluster itself, but complicates any interpretation of the red sequence build-up in MRC 0943–242 until more redshifts can be measured.

**Key words.** Galaxies: clusters: individual: MRC 1138–262 – Galaxies: clusters: individual: MRC 0943–242 – Galaxies: evolution – Galaxies: high-redshift – (Cosmology:) large-scale structure of Universe – Infrared: galaxies

## 1. Introduction

At every epoch, galaxies with the reddest colours are known to trace the most massive objects (Tanaka et al. 2005). The study of massive galaxies at high redshift therefore places important constraints on the mechanisms and physics of galaxy formation (e.g., Hatch et al. 2009). Studies of clusters at both low and high redshift also yield valuable insights into the assembly and evolution of large-scale structure, which itself is a sensitive cosmological probe (e.g., Eke et al. 1996).

The most distant spectroscopically confirmed cluster lies at  $z = 1.45$  and has 17 confirmed members, a large fraction of which are consistent with massive, passively evolving ellipticals (Stanford et al. 2006; Hilton et al. 2007). High redshift proto-clusters have been inferred through narrow-band imaging

searches for Ly- $\alpha$  emitters in the vicinity of radio galaxies (e.g., Kurk et al. 2004a; Venemans et al. 2005). Such searches have been highly successful, with follow-up spectroscopy confirming 15 – 35 Ly- $\alpha$  emitters per proto-cluster. However, the Ly- $\alpha$  emitters are small, faint, blue star-forming galaxies, and likely constitute a small fraction of both the number of cluster galaxies and the total mass budget in the cluster.

Massive elliptical galaxies are seen to dominate cluster cores up to a redshift of  $z \approx 1$  (e.g., van Dokkum et al. 2001), with the red sequence firmly in place by that epoch (Ellis et al. 2006; Blakeslee et al. 2003) and in fact showing very little evolution even out to  $z \sim 1.4$  (e.g., Lidman et al. 2008). What remains uncertain is whether this holds true at yet higher redshift. The fundamental questions are (1) at what epoch did massive, rich clusters first begin to assemble, and (2) from what point do they undergo mostly passive evolution? There is certainly evidence that the constituents of high redshift clusters are very different from that of rich clusters in the local Universe, with the distant clusters containing a higher fraction of both blue spirals (e.g., Ellis et al. 2006) and active galaxies (Galametz et al.

<sup>★</sup> Based in part on data collected at Subaru Telescope, which is operated by the National Astronomical Observatory of Japan, and in part on data collected with ESO's Very Large Telescope UT1/Antu, under program ID 080.A-0463(B), and ESO's New Technology Telescope under program ID 076.A-0670(B)

2009). van Dokkum & Stanford (2003) found early-type galaxies with signatures of recent star formation in a  $z = 1.27$  cluster, perhaps symptomatic of a recently formed (or still forming) cluster. Locating massive galaxies in higher redshift clusters will therefore yield valuable insight into the earliest stages of cluster formation and the build-up of complex structures which are observed in the local Universe.

In two previous papers, we found over-densities of red colour-selected galaxies in several proto-clusters associated with high redshift radio galaxies (Kajisawa et al. 2006; Kodama et al. 2007). Follow up studies of distant red galaxies (DRGs) have shown that this colour selection criterion contains two populations: (1) dusty star-forming galaxies and (2) passively evolved galaxies. The exact fraction between these two populations is still a matter of debate (Förster Schreiber et al. 2004; Grazian et al. 2006, 2007). With our new *JHK* colour-selection, we hope to be more efficient in identifying the evolved galaxy population. We have now embarked upon a spectroscopic follow-up investigation with the aim of confirming cluster members and determining their masses and recent star formation histories. Such a goal is ambitious as redshifts of these red galaxies are generally very difficult to obtain, especially amongst the population with no on-going star formation (i.e., lacking emission lines). Here we present the first results from optical and near-infrared spectroscopy of targets in two of the best studied proto-clusters, MRC 1138–262 ( $z = 2.16$ ) and MRC 0943–242 ( $z = 2.93$ ).

In Section 2 we explain the target selection and in Section 3 outline the observations and data reduction steps. Section 4 presents the redshifts identified and in Section 5 we briefly analyse the properties of the two galaxies discovered at the redshift of MRC 1138–262, including their relative spatial location to the RG, ages, masses and star formation rates from spectral energy distribution fits and star formation rates from the  $H\alpha$  emission line flux. In Section 6 we summarise the results and draw some wider conclusions.

Throughout this paper we assume a cosmology of  $H_0 = 71 \text{ km s}^{-1}$ ,  $\Omega_M = 0.27$ ,  $\Omega_\Lambda = 0.73$  (Spergel et al. 2003) and magnitudes are on the Vega system.

## 2. Target selection

### 2.1. Proto-clusters

We have concentrated the initial stages of our spectroscopic campaign on MRC 1138–262 and MRC 0943–242 for several reasons. First, these two proto-clusters fields were both observed in the space infrared by a *Spitzer* survey of 70 high redshift radio galaxies (RGs; Seymour et al. 2007). They are also amongst the eight  $z > 2$  radio galaxies observed in the broad and narrow-band imaging survey of Venemans et al. (2007). Both targets therefore are among the best studied high-redshift radio galaxies and have a large quantity of broadband data available from the *U*-band to the *Spitzer* bands, over a wide field of view. Their redshifts span the  $2 < z < 3$  region in which it has been shown that the red sequence most likely starts to build up Kodama et al. (2007), and they therefore probe an interesting and poorly understood redshift regime for understanding the build-up of red, massive galaxies in proto-clusters.

Our group previously obtained deep, wide-field near-infrared imaging of MRC 1138–262 and MRC 0943–242 with the Multi-Object InfraRed Camera and Spectrograph (MOIRCS; Suzuki et al. 2008; Ichikawa et al. 2006), the relatively new  $4' \times 7'$  imager on Subaru (Kodama et al. 2007). The data were ob-

tained in exceptional conditions, with seeing ranging from  $0''.5$  to  $0''.7$ . We use our previously published photometric catalogues, and quote the total magnitudes (MAGAUTO in SExtractor) for individual band photometry, and  $1.5''$  diameter aperture magnitudes for all colours. We refer to (Kodama et al. 2007) for further details on the photometry. We also used an *H*-band image of MRC 1138–262 obtained with the Son of ISAAC (SOFI) on the New Technology Telescope (NTT) on UT 2006 March 23. The total exposure time was 9720 s. We reduced the data using the standard procedures in IRAF.

Using this data set, we selected galaxies expected to lie at the same redshifts as the radio galaxies on the basis of their  $J - K_s$  or  $JHK_s$  colours. These deep data indicate a clear excess of the near-infrared-selected galaxies clustered towards the radio galaxies (e.g., Figures 3–5 in Kodama et al. 2007). The excess is a factor of  $\approx 2 - 3$  relative to the GOODS-S field.

### 2.2. MRC 1138–262 at $z = 2.16$

The red galaxies in MRC 1138–262 were selected according to the ‘classic’ DRG criterion of  $J - K_s > 2.3$  (van Dokkum et al. 2004). We note that in Kodama et al. (2007) the zero points of the photometry in this field were incorrect by 0.25 and 0.30 magnitudes in *J* and *K<sub>s</sub>* bands, respectively, with  $J' = J - 0.25$ ,  $K'_s = K_s - 0.30$  for this field, where the primed photometry represents the corrected values. Since the corrections for both bands are similar, there is little change in the sample of DRGs identified, which was the primary thrust of that paper. We have adjusted the magnitudes and colours before revising the target selection for the current paper. We also include three near-infrared spectroscopic targets in the field of MRC 1138–262 from the *Hubble Space Telescope* NICMOS imaging reported by Zirm et al. (2008), two of which fulfill the DRG criterion and one of which is slightly bluer. We targeted 33 red galaxies in this field, down to a *K<sub>s</sub>* magnitude of 21.7.

### 2.3. MRC 0943–242 at $z = 2.93$

For the redshift  $z \sim 3$  proto-cluster MRC 0943–242, we define two classes of colour-selected objects: blue *JHK<sub>s</sub>* galaxies (bJHKs) defined to have:

$$J - K_s > 2(H - K_s) + 0.5 \text{ and } J - K_s > 1.5,$$

and red *JHK<sub>s</sub>* galaxies (rJHKs) defined to have:

$$J - K_s > 2(H - K_s) + 0.5 \text{ and } J - K_s > 2.3.$$

Figure 1 shows these colour cuts and the objects which were targeted for spectroscopy. Note that although we have not used *H*-band data in the selection of targets for MRC 1138–262, we include a *JHK<sub>s</sub>* diagram for that field as a comparison to MRC 0943–242 - it is obvious from these diagrams that the two colour cuts select distinct populations of objects.

Figure 2 demonstrates how our *JHK<sub>s</sub>* selection works to select candidate proto-cluster members around MRC 0943–242. The solid curves represent the evolutionary tracks of galaxies over  $0 < z < 4$  with different star formation histories (passive, intermediate, and active) formed at  $z_{\text{form}} = 5$  (Kodama et al. 1999). The dashed line connects the model points at  $z = 3$ , and indicates the region where we expect to find galaxies at a similar redshift to the radio galaxy. We therefore apply the colour-cut (shown by the dot-dashed lines) to exclusively search for galaxies associated with the radio galaxies at  $2.3 < z < 3.1$ . This technique was originally used by Kajisawa et al. (2006) and has a great advantage over the DRG selection used at lower redshift since we also select the bluer populations within the redshift range of interest.

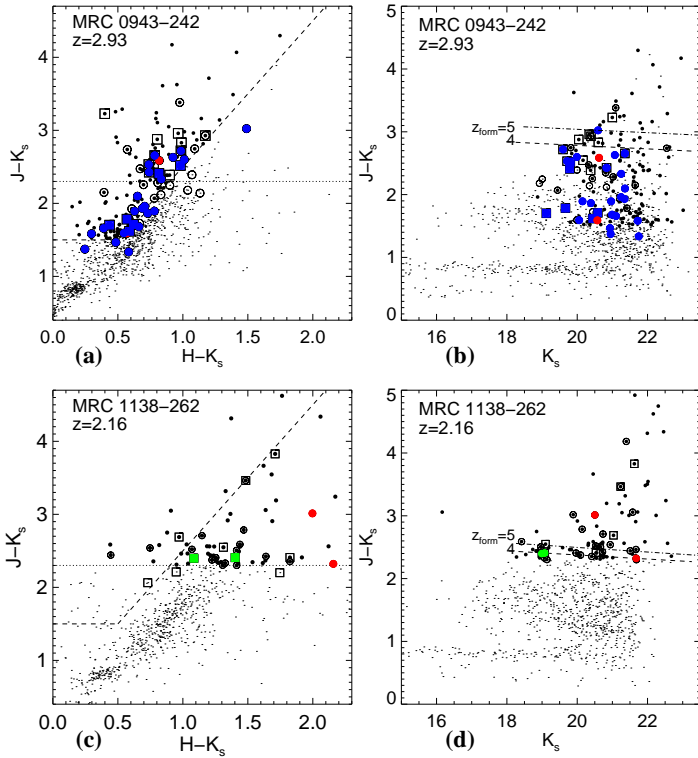


**Fig. 1.** Spectroscopic targets shown in colour-colour (left) and colour-magnitude (right) space for MRC 0943–242 (top) and MRC 1138–262 (bottom). Objects observed with optical spectroscopy by either FORS2 or FOCAS are indicated by large circles; objects observed with near-infrared spectroscopy by MOIRCS are indicated by squares. With respect to the radio galaxy, filled blue symbols are confirmed foreground objects and red filled symbols are background galaxies. Green symbols show galaxies confirmed to lie at the redshift of the radio galaxy.

We targeted 38  $JHK_s$  selected galaxies (including the RG itself) down to a magnitude  $K_s = 22$ . In section 4.1, we will show that we could measure redshifts of half of these sources with a success rate of our selection technique of  $\sim 55\%$ . In the remaining spectroscopic slits, we included 22 additional “filler” targets (see Table 2), mostly those with colours just outside our selection criterion, but also two Distant Red Galaxies ( $J - K > 2.3$ ) and three Ly $\alpha$  emitters.

Where two or more objects clashed in position, we prioritised objects with  $24\mu\text{m}$  detections from the Multiband Imaging Photometer for *Spitzer* (MIPS; Rieke et al. 2004). For the optical spectroscopy, we also prioritised objects with brighter  $I$ -band magnitudes. After selecting primary targets according to the above colour criteria, a couple of additional ‘filler’ targets were selected depending on the geometry of the mask. These filler objects were drawn from a list of candidate Ly $\alpha$  emitters which do not yet have confirmed redshifts (Venemans et al. 2007). Figure 1 shows the distribution of selected targets in colour-colour and colour-magnitude space. Whilst by no means complete sample, we believe our sample to be representative of the candidate objects.

### 3. Observations and data reduction

We obtained optical multi-object spectra of targeted galaxies in the two proto-clusters using the Faint Object Camera and

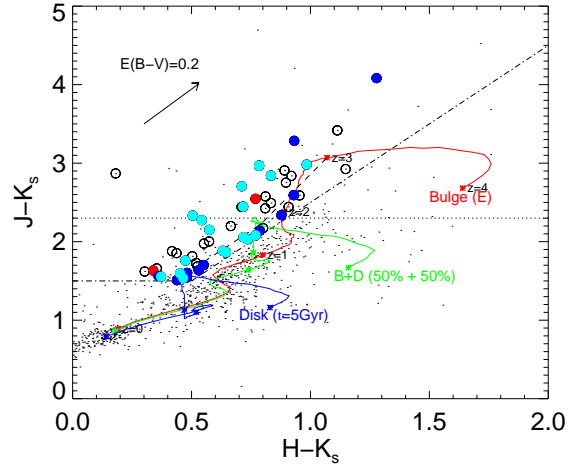


**Fig. 2.** Colour selection technique designed to select galaxies at  $2.3 < z < 3.1$ . The solid curves represent the evolutionary tracks of galaxies over  $0 < z < 4$  with different star formation histories (passive, intermediate, and active, from top to bottom, respectively) formed at  $z_{\text{form}} = 5$  (Kodama et al. 1999). The dashed line connects the model points at  $z = 3$ . Objects targeted spectroscopically are represented by circles; filled circles indicate where a redshift identification has been made. Blue circles indicate objects at  $z < 2.3$  and red circles indicate sources at  $z > 3.1$  — i.e., outside of the targeted redshift range. Cyan circles show objects whose redshifts fall within the targeted range.

Spectrograph (FOCAS; Kashikawa et al. 2000) on Subaru, and the FOCal Reducer and low dispersion Spectrograph-2 (FORS2; Appenzeller & Rupprecht 1992) on the VLT<sup>1</sup>. We obtained near-infrared multi-object spectra of targeted galaxies using MOIRCS on Subaru. For one galaxy, we also obtained a spectrum with X-SHOOTER (D’Odorico et al. 2006) on the VLT during a commissioning run. A summary of the observations is presented in Table 1.

#### 3.1. Optical spectra

We were scheduled two nights, UT 2007 March 14–15, of FOCAS spectroscopy on Subaru. However, 1.5 out of the two nights were lost to bad weather. In the first half of the second night, we obtained three hours integration on MRC 0943–242 in variable seeing. We used the 300B grism with the L600 filter and binned the readout  $3 \times 2$  (spatial  $\times$  spectral). This set-up gives a dispersion of  $1.34 \text{ \AA pix}^{-1}$  and a spectral resolution of  $9 \text{ \AA}$  full width at half maximum (FWHM; as measured from sky lines). There were 22 slits on the mask, but the spectra for three objects fell on bad CCD defects so we treat these as unobserved. Two Ly $\alpha$  emitter candidates were also placed on the mask to fill in space where there were no suitable near-infrared selected galaxies. The data were reduced in a standard manner using IRAF and custom software. Although the night was not photometric, spectra were flux calibrated with standard stars observed on the same night, as it is important to calibrate at least the relative spectral response given that we are interested in breaks across the spectra.

We obtained FORS2/MXU spectra with UT2/Kueyen on UT 2008 March 11–12. The nights were clear with variable seeing averaging around  $1''$ . The 300V grating was used, providing a

<sup>1</sup> ESO program 080.A-0463(B).

dispersion of  $3.36 \text{ \AA pix}^{-1}$  and a resolution of  $12 \text{ \AA}$  (FWHM, measured from sky lines). Slitlets were  $1''$  wide and  $6\text{--}10''$  long. We used  $2''$  nods to shift objects along the slitlets, thereby creating A-B pairs to improve sky subtraction. We first created time-contiguous pairs of subtracted frames, and then averaged all of the A-B pairs together in order to improve the resulting sky subtraction and to reject cosmic rays (in both the positive and negative images). These combined frames were then processed using the FORS2 pipeline (ver. 3.1.7) with standard inputs. The extracted one-dimensional spectra were boxcar extracted over a  $1''$  aperture and calibrated with flux standards taken on the same night. In total, we obtained 10 hours of integration on MRC 0943–242 and five hours of integration on MRC 1138–262.

### 3.2. Near-infrared spectra

We obtained MOIRCS spectra for MRC 1138–262 over the latter halves of UT 2008 January 11–12. Both nights were photometric, and we obtained a total of five hours of integration. Since Chip 1 of MOIRCS was the engineering grade chip at that time, we gained no useful data on that chip and essentially lost half of the field coverage. This detector suffered a loss of sensitivity compared to chip 2. More problematic was a prominent large ring-like structure with significantly high (and variable) dark noise, as well as several smaller and patchy structures, which we were unable to calibrate out successfully. We obtained  $K$ -band spectra with the medium resolution (R1300) grating, yielding a dispersion of  $3.88 \text{ \AA pix}^{-1}$  and a resolution of  $26 \text{ \AA}$  (FWHM, measured from sky lines). The objects were nodded along the slitlets and A-B pairs combined to remove the sky background. The frames were then flat-fielded and corrected for optical distortion using the `mscgeocorr` task in IRAF. They were then rotated to correct for the fact that the slits are tilted on the detector. We extracted spectra using a box-car summation over the width of the continuum, or, in the case of no continuum, over the spatial extent of any detected line emission.

We obtained MOIRCS data for MRC 0943–242 on UT 2009 January 10, with four hours total integration time over the latter half of the night. The low resolution HK500 grating was used, providing a dispersion of  $7.72 \text{ \AA pix}^{-1}$  and a resolution of  $42 \text{ \AA}$  (FWHM, measured from sky lines).

### 3.3. UV/Optical/NIR spectrum

We also obtained data for a single target in the field of MRC 0943–242 with X-SHOOTER during a commissioning run on 2009 June 5 under variable seeing conditions (between  $0.5''$  and  $2''$  during the exposure). Slit widths of  $1.0''$ ,  $0.9''$  and  $0.9''$  were used in the UV-blue, visual-red and near-IR arm, respectively, resulting in resolutions of  $R_{\text{UVB}}=5100$ ,  $R_{\text{VIS}}=8800$  and  $R_{\text{NIR}}=5100$ . The data were reduced using a beta version of the pipeline developed by the X-SHOOTER consortium (Goldoni et al. 2006). The visual-red arm spectrum (550nm–1000nm) presented below is a combination of three 1200s exposures. The near-IR arm spectrum (1000nm–2500nm) is a combination of two 1300s exposures in a nodding sequence.

## 4. Results/redshift identifications

Redshifts were identified by visual inspection of both the processed, stacked two-dimensional data and the extracted, one-dimensional spectra. We based redshifts on both emission and

absorption line features, as well as possible continuum breaks and assigned confidence flags.

Table 2 shows the sources observed with optical spectroscopy and the corresponding redshift identifications and quality flags. Quality 1 indicates confirmed, confident redshifts; quality 2 indicates doubtful redshifts; quality 3 indicates that we detected continuum emission but no identification was made, typically due to the low signal-noise ratio (S/N) of the data; and quality 4 indicated that no emission was detected. In some cases we can infer an upper limit to the redshift if the continuum extends to the blue wavelength cutoff of the optical spectrum. This is useful for distinguishing foreground objects. In practice, due to the lower efficiency of the grisms, the spectra become too noisy to distinguish the continuum below  $3900 \text{ \AA}$  for FORS and  $4100 \text{ \AA}$  for FOCAS, corresponding to  $\text{Ly-}\alpha$  at  $z=2.3$  and  $z=2.4$ , respectively.

### 4.1. MRC 0943–242

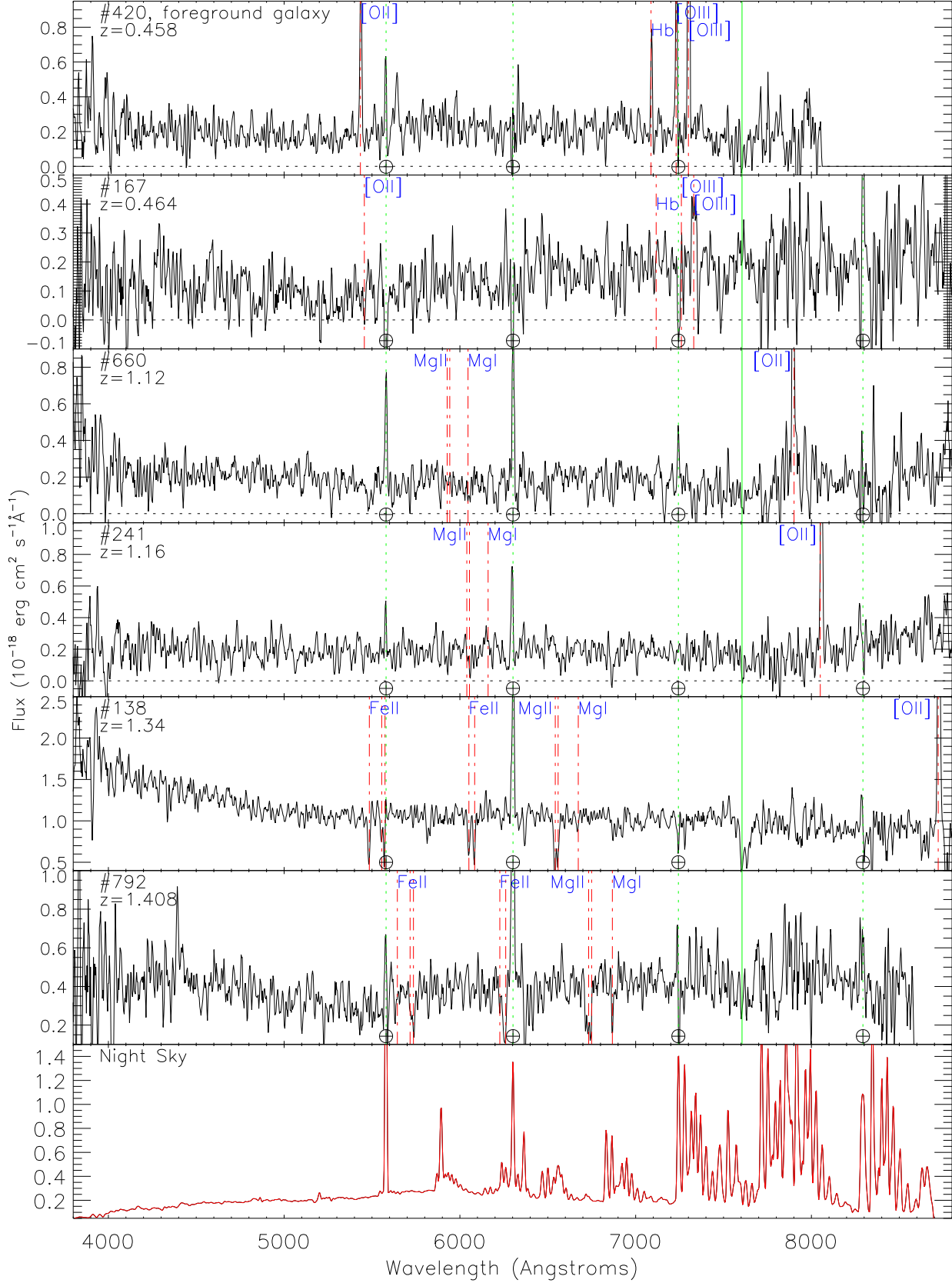
Out of 32 objects observed with FORS2 in MRC 0943–242, 16 redshifts have been identified (Fig. 3). Nineteen objects were observed with FOCAS, including 17 near-infrared-selected galaxies and two  $\text{Ly-}\alpha$  candidates observed as filler objects (Fig. 4). We obtained five redshifts, only one of which lies close to the redshift of the radio galaxy, LAE#381 at  $z = 2.935$  (Quality 1) and this is not one of our red galaxy candidate members but was one of the Lyman-alpha emitter candidates. The low success rate with FOCAS is most likely due to the short exposure time since that observing run was largely weathered out.

We identified a further 8 redshifts with MOIRCS (out of 21 targeted sources), giving a total of 27 sources in the field of MRC 0943–242 with spectroscopic redshifts, out of 57 targeted (Fig. 5).

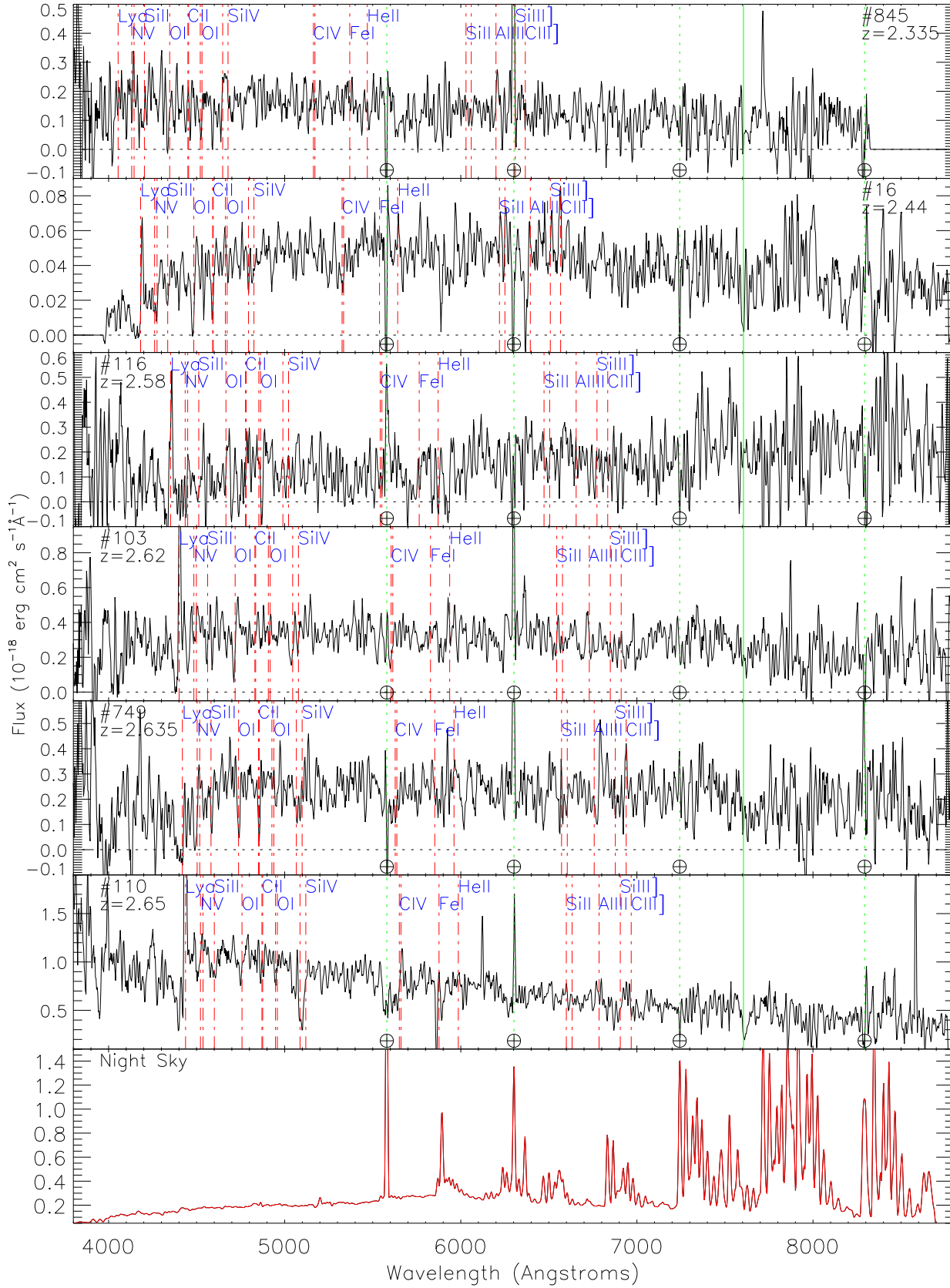
We also observed one object (#792) with X-SHOOTER. The visual-red arm spectrum (Fig. 6) shows one line at  $8985.7 \text{ \AA}$ . The near-IR arm spectrum (Fig. 7) shows two lines at  $15815.7 \text{ \AA}$  and  $15868.2 \text{ \AA}$ . We identify those lines as  $[\text{OII}]\lambda 3727$ ,  $\text{H}\alpha$  and  $[\text{NII}]\lambda 6583$  at  $z=1.410$ . This redshift is consistent with the one determined independently from the spectrum obtained with FORS.

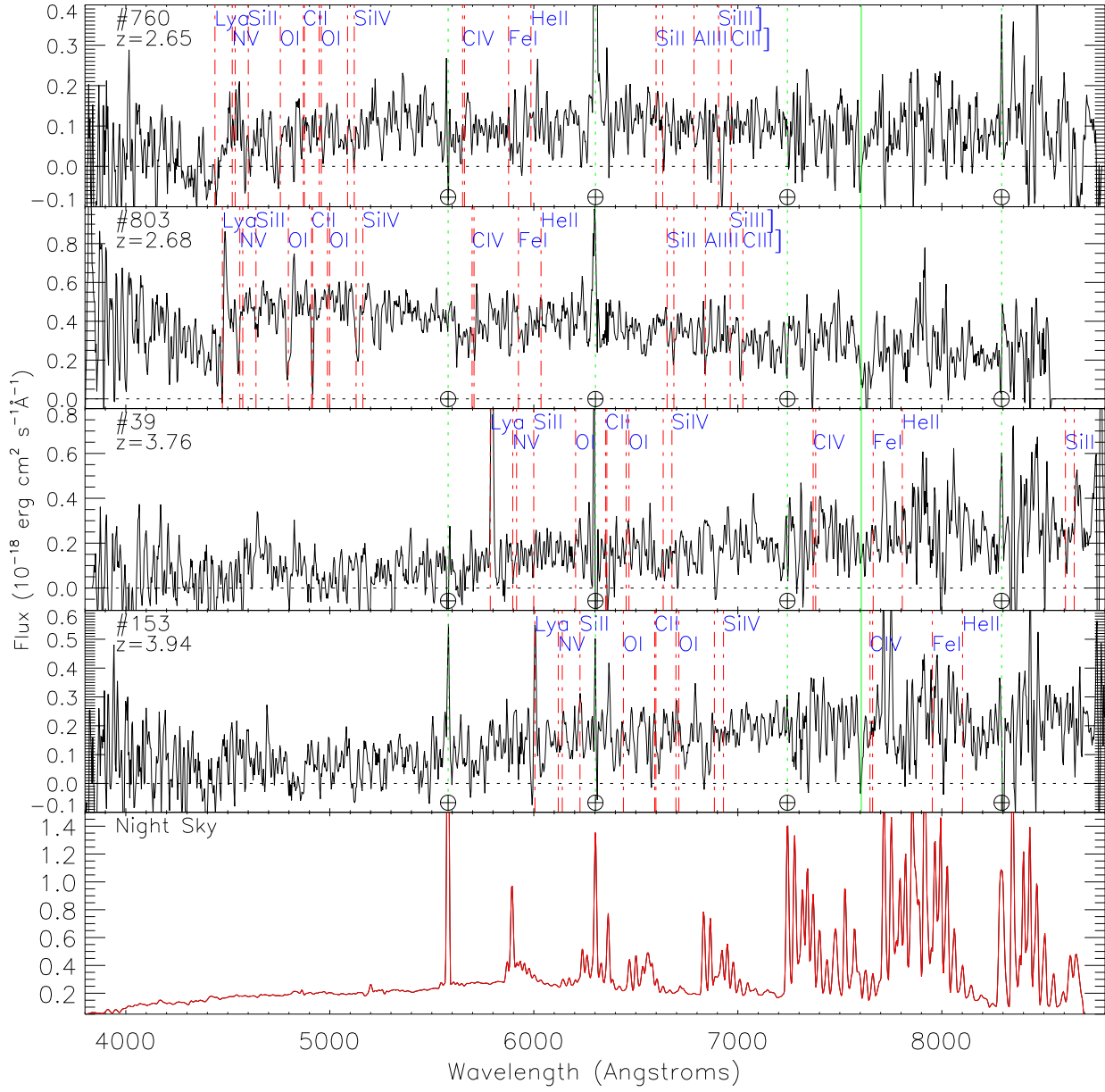
From the remaining 30 sources, we obtained five redshift upper limits from the optical spectroscopy, excluding these sources from being members of the proto-cluster. The remaining 25 objects cannot be excluded as either foreground or background objects, and an unknown fraction of these may even be at the redshift of the radio galaxy. However, we found an extended foreground structure in this field at redshift  $z \sim 2.6$ . The redshift distribution is shown in Figure 8. This foreground structure complicates any interpretation of the red sequence, or lack thereof, in this proto-cluster, as a large number of galaxies along the ‘red sequence’ in MRC 0943–242 may be members of this intervening structure. However, it is in itself very interesting as it lies at a high redshift and may also be a young, forming cluster. We find six galaxies in this structure, with a mean redshift  $\langle z \rangle = 2.65$  and  $\Delta z = 0.03$ . Several of these sources may contain AGN features (CIV, HeII lines), though the S/N of our spectra is insufficient to make a clear statement about this.

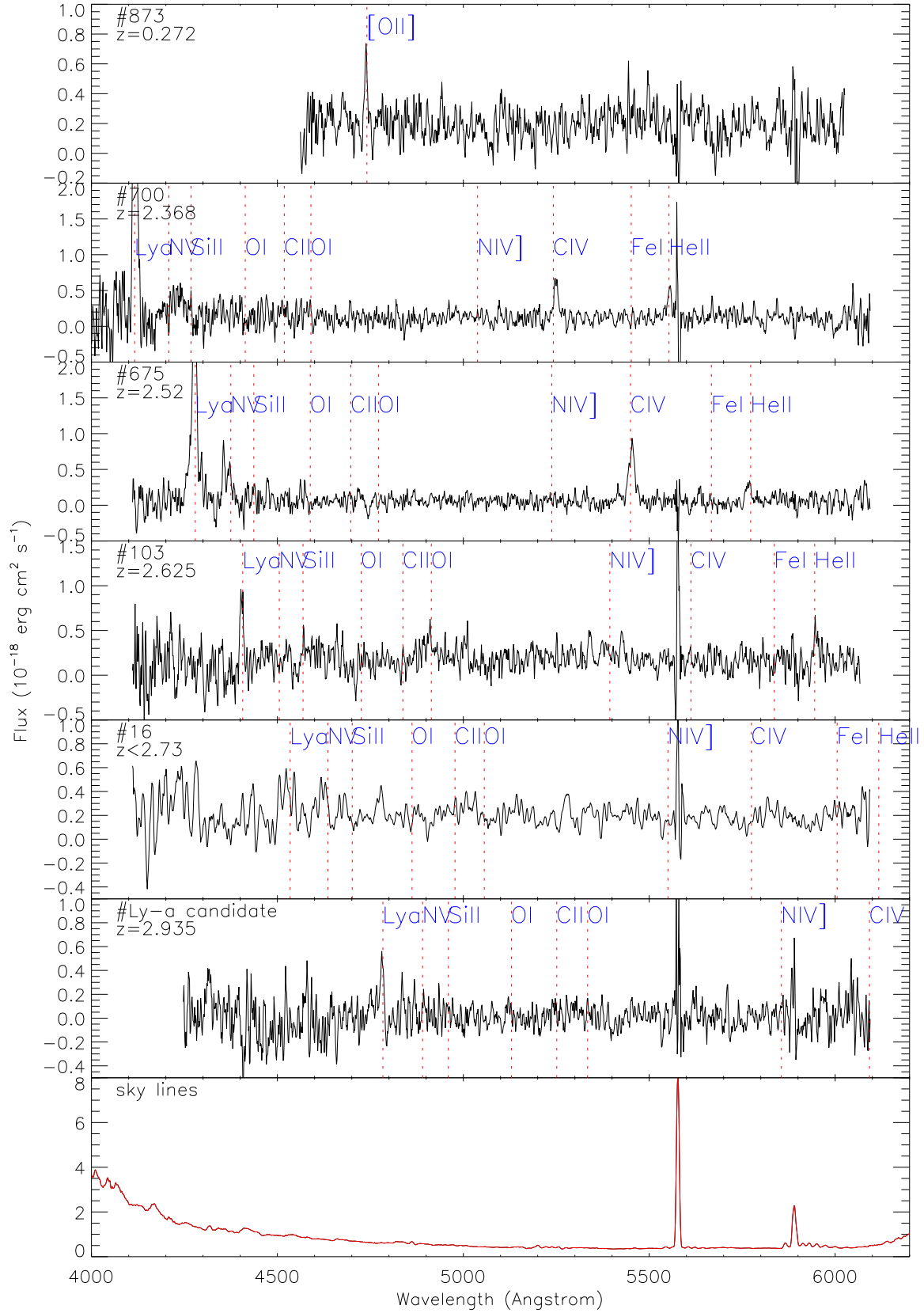
For one object, #420, we obtained two different redshifts from FORS2 and MOIRCS. Upon closer inspection of the  $I$ -band and  $K$ -band images, we found out that this is actually a pair of galaxies: (i) a blue one at  $z = 0.458$  detected in the  $I$ -band image, and used to centre our FORS2 spectroscopic slit (Fig. 3), and (ii) a red one at  $z = 2.174$  detected in the  $K$ -band image and



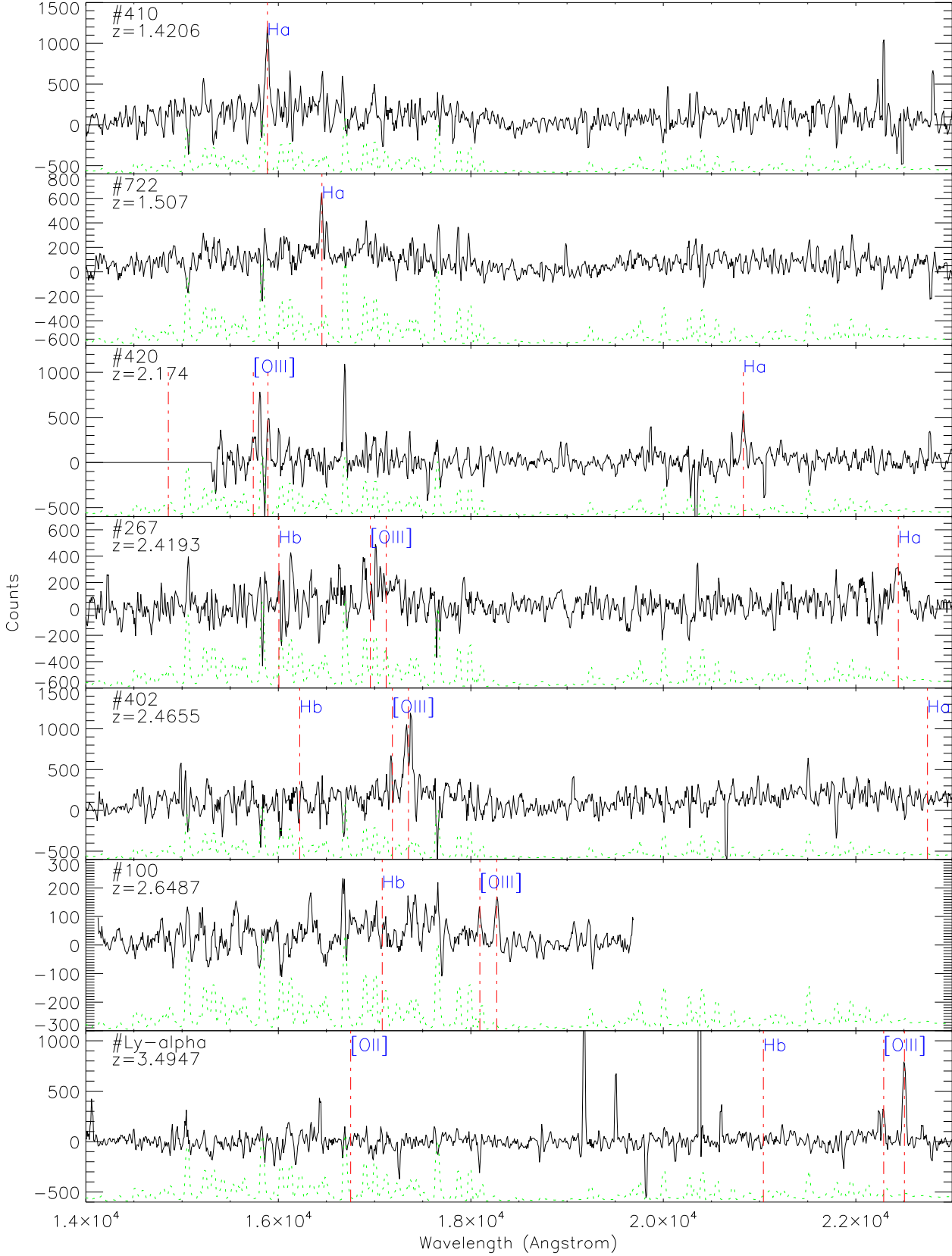
**Fig. 3.** FORS2 spectra of objects with identified redshifts in the field of MRC 0943–242. Objects are ordered by redshift from low to high. The vertical green line indicates the region of atmospheric absorption at 7600 Å. The horizontal dashed line indicates zero

Fig. 3. *cont.*

Fig. 3. *cont.*



**Fig. 4.** FOCAS spectra of objects with identified spectra in the field MRC 0943–242.

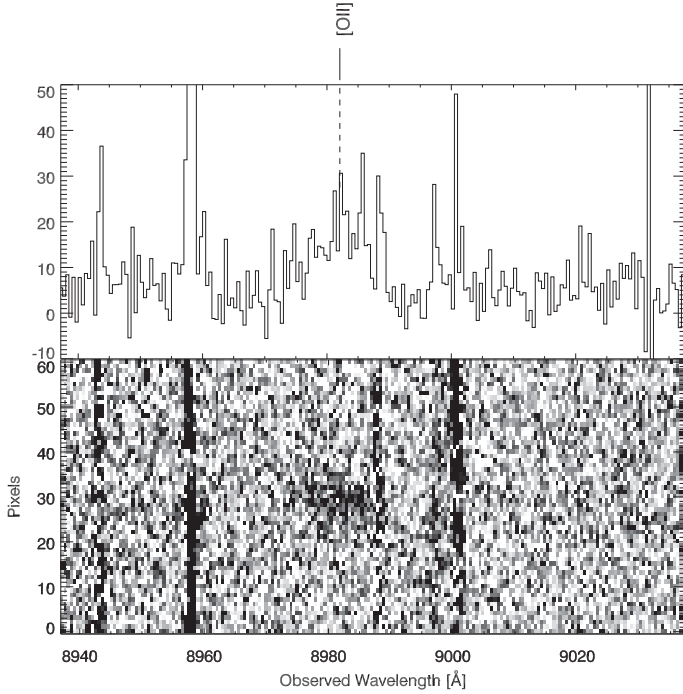


**Fig. 5.** MOIRCS spectra of objects with identified redshifts in the field MRC 0943–242. Sky lines are shown as a dotted green spectrum beneath each object spectrum.

**Table 1.** Summary of observations.

Proto-cluster	Instrument	FOV	Filter	Grating	Spectral Coverage <sup>a</sup> ( $\mu\text{m}$ )	UT Date Obs.	Total Exp.
MRC 1138–262	MOIRCS	$4' \times 3.5'$	<i>K</i>	R1300	2.0 – 2.4	11–12 Jan 2008	5 hr
MRC 1138–262	FORS2	$7' \times 7'$	–	300V	0.33 – 0.9	11–12 Mar 2008	5 hr
MRC 0943–242	FORS2	$7' \times 7'$	–	300V	0.33 – 0.9	11–12 Mar 2008	10 hr
MRC 0943–242	FOCAS	$6'$ diameter	L600	300B	0.37 – 0.6	15 Mar 2007	3 hr
MRC 0943–242	MOIRCS	$4' \times 7'$	OC_HK	HK500	1.3 – 2.5	10 Jan 2009	4 hr
MRC 0943–242	X-SHOOTER	$1'' \times 11''$	–	–	0.3 – 2.5	5 Jun 2009	1 hr

<sup>a</sup> Exact spectral coverage for each object depends on the position of the slit on the detector.

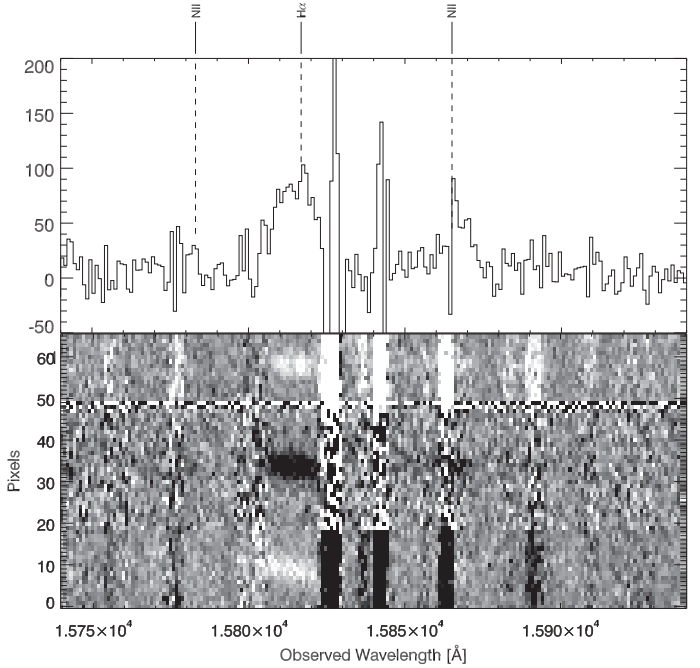
**Fig. 6.** X-SHOOTER visual-red arm spectrum of object #792 in the field of MRC 0943–242.

used to centre the MOIRCS slit (Fig. 5). These two galaxies are separated by only  $1''.1$ . A hint of the blue galaxy is seen in the *K*-band image, and vice versa, a hint of the red galaxy is seen in the *I*-band image, but none of these can be properly deblended. The red galaxy at  $z = 2.174$  is the one selected by our colour criterion.

More than a half (10/18, or 56%) of the *JHK<sub>s</sub>* selected galaxies whose redshifts were successfully measured turn out to be actually located in the redshift range  $2.3 < z < 3.1$ . Of the red sequence candidates (i.e., rJHK galaxies), 6 out of 10 are within the range  $2.3 < z < 3.1$ . These numbers are summarised in Table 4. The majority of redshift identifications were based on emission lines, though in several cases the FORS2 data yielded absorption line identifications where the continuum is strong enough (e.g., see objects #749 and #760 in Figure 3).

#### 4.2. MRC 1138–262

We observed 27 objects (25 red galaxies and 2  $L\alpha$  emitters) in the MRC 1138–262 field with optical spectroscopy, but could identify only two redshifts, both of which are background  $L\alpha$  emitters at  $z > 3$  (Figure 9). No redshifts were confirmed at the

**Fig. 7.** X-SHOOTER NIR arm spectrum of object #792 in the field of MRC 0943–242.

redshift of the radio galaxy from optical spectroscopy. Although the total exposure time is half of that spent on MRC 0943–242, given the 50% confirmation rate in that field we may naively expect a higher success rate here given the lower redshift of this radio galaxy. However, about twice as many sources (25 out of 57) in the MRC 0943–242 field have  $I < 24.5$ , compared to the MRC 1138–262 field (7 out of 33), so the lower success rate in MRC 1138–262 may be partially due to the sources being fainter. We are confident that the astrometry in both masks is accurate — confirmed by several stars and bright galaxies (including the radio galaxy itself) placed on the slitmasks. The astrometry was internally consistent as the slit positions were derived from preimaging obtained with FORS2. However, the efficiency of the 300V grism drops off quickly at the blue end, and since the sources observed in this field have such faint magnitudes, it is likely not possible to detect Lyman breaks at the redshift of the radio galaxy; we estimate a minimum redshift of  $z = 2.2$  to detect  $L\alpha$  with FORS2, and the sources were too faint to identify redshifts from absorption lines. Furthermore, given the difference in colour cuts from MRC 0943–242 which selects intrinsically different populations (Figure 1), we do not expect to find many higher redshift interlopers.



**Table 3.** Results of optical and near-IR spectroscopy in the MRC 1138–262 field.

ID	RA(J2000)	Dec.(J2000)	$B_{total}$	$I_{total}$	$J_{total}$	$K_{s,total}$	$J - K_s$ (1''5)	Instr.	$z$	Quality <sup>a</sup>
493	11 40 33.42	-26 29 14.6	>27	>26.2	22.89	20.55	2.56	FORS2	...	4
867	11 40 34.09	-26 30 38.7	>27	25.32	>23.3	21.30	2.49	FORS2	...	4
156	11 40 34.82	-26 27 46.4	>27	>26.2	>23.3	21.15	4.23	FORS2	...	4
174	11 40 35.45	-26 27 51.8	25.35	25.06	>23.3	>22	2.51	FORS2	...	3
676	11 40 36.96	-26 29 55.6	>27	>26.2	22.57	19.79	3.07	FORS2	...	4
808	11 40 38.19	-26 30 24.3	>27	24.87	22.91	20.44	2.56	FORS2	...	4
552	11 40 38.28	-26 29 25.1	>27	25.37	22.67	20.47	2.41	MOIRCS	...	4
364	11 40 39.76	-26 28 45.4	24.17	22.87	21.24	19.03	2.21	MOIRCS	...	3
877	11 40 40.24	-26 30 41.2	25.96	24.91	23.44	21.30	2.35	FORS2	...	3
341	11 40 41.47	-26 28 37.2	>27	24.81	23.63	20.48	3.06	FORS2	3.263	1
147	11 40 43.48	-26 27 44.1	>27	>26.2	21.98	20.04	2.43	FORS2	...	3
369	11 40 43.46	-26 28 45.2	>27	>26.2	>23.3	21.30	3.83	MOIRCS	...	4
905	11 40 44.01	-26 30 47.0	>27	>26.2	23.45	20.86	2.69	MOIRCS	...	4
456	11 40 44.28	-26 29 07.7	>27	24.71	21.28	18.93	2.45	FORS2	...	3
								MOIRCS	2.172	2
464	11 40 46.09	-26 29 11.5	>27	>26.2	21.54	19.06	2.41	MOIRCS	2.149	2
558	11 40 46.52	-26 29 27.1	>27	24.71	21.64	19.03	2.55	MOIRCS	...	4
476	11 40 46.68	-26 29 10.4	>27	24.90	22.30	19.86	2.46	FORS2	...	3
605	11 40 47.58	-26 29 38.2	>27	>26.2	>23.3	21.07	3.51	FORS2	...	4
								MOIRCS	...	4
830	11 40 48.36	-26 30 30.6	>27	20.48	20.67	18.86	2.20	MOIRCS	...	3
492	11 40 49.59	-26 29 07.7	>27	25.60	23.09	20.02	2.84	FORS2	...	4
392	11 40 50.35	-26 28 49.6	>27	>26.2	23.47	20.56	2.47	FORS2	...	4
573	11 40 50.75	-26 29 32.5	>27	24.68	21.98	20.04	2.06	MOIRCS	...	4
601	11 40 51.30	-26 29 38.5	>27	23.45	21.27	19.05	2.35	FORS2	...	3
506	11 40 53.13	-26 29 18.1	>27	23.55	21.33	19.01	2.38	FORS2	...	3
165	11 40 54.01	-26 27 48.1	>27	>26.2	23.35	20.85	2.59	FORS2	...	4
241	11 40 54.77	-26 28 03.6	>27	25.44	23.16	20.78	2.76	FORS2	...	3
223	11 40 55.99	-26 28 02.9	26.13	24.30	>23.3	21.36	2.37	FORS2	3.455	1
268	11 40 57.02	-26 28 17.5	>27	23.02	20.57	18.35	2.64	FORS2	...	3
206	11 40 57.87	-26 27 59.3	>27	24.52	23.51	20.28	2.40	FORS2	...	3
565	11 41 00.10	-26 29 28.1	>27	>26.2	22.72	20.31	2.57	FORS2	...	4
451	11 41 00.84	-26 29 04.7	>27	>26.2	>23.3	21.26	3.11	FORS2	...	4
90	11 41 01.54	-26 27 31.2	>27	23.55	21.38	18.89	2.51	FORS2	...	3
728	11 41 02.69	-26 30 07.8	>27	>26.2	21.03	18.89	2.56	FORS2	...	4
...	11 40 43.85	-26 31 26.4		Ly- $\alpha$ emitter candidate				FORS2	...	3
...	11 40 50.68	-26 31 00.0		Ly- $\alpha$ emitter candidate				FORS2	...	4

<sup>a</sup>Quality flags are the same as in Table 2. Limiting magnitudes are  $5\sigma$ .**Table 4.** Spectroscopy summary for near-IR selected candidates.

Selection Criterion	# Candidates	# Targeted	# Confirmed Redshifts	# @ $2.3 < z < 3.1$	# @ $z_{RG}$
MRC 0943–242					
rJHK	62	23	10	6	0
bJHK	70	15	8	4	1 <sup>a</sup>
Total	132	38	18	10	1 <sup>a</sup>
MRC 1138–262					
DRG	97	30	15	4	2

<sup>a</sup> This is the radio galaxy itself, which is also selected as a bJHK candidate.

From the MOIRCS spectra, we detected two emission line objects (out of 12 targets), which, if identified as H $\alpha$ , places the objects at the same redshift as the radio galaxy. One of these is a clear detection, the other is marginal ( $3\sigma$ ). Both the two-dimensional and extracted one-dimensional spectra are shown in Figures 10 and 11. The target information for these two objects are shown in Table 3.

The small number of confirmed redshifts in this field is in fact not surprising given that detecting interstellar absorption lines and the Lyman-break in the optical was unsuccessful. As we seem to detect only a surprisingly low number of star-forming red galaxies in our colour-selection, the remaining frac-

tion of passively evolving red sequence galaxies will not have strong emission lines, and hence will be harder to confirm redshifts of. Our current results show that the most effective strategy would in fact be to observe much deeper in the near-IR so that we can detect the 4000Å continuum break feature, if present (e.g., Kriek et al. 2006). In fact, there are a total of 13 objects in which we detect continuum in our near-IR spectra, but in general it is too weak and/or diffuse to identify any features with the current data.

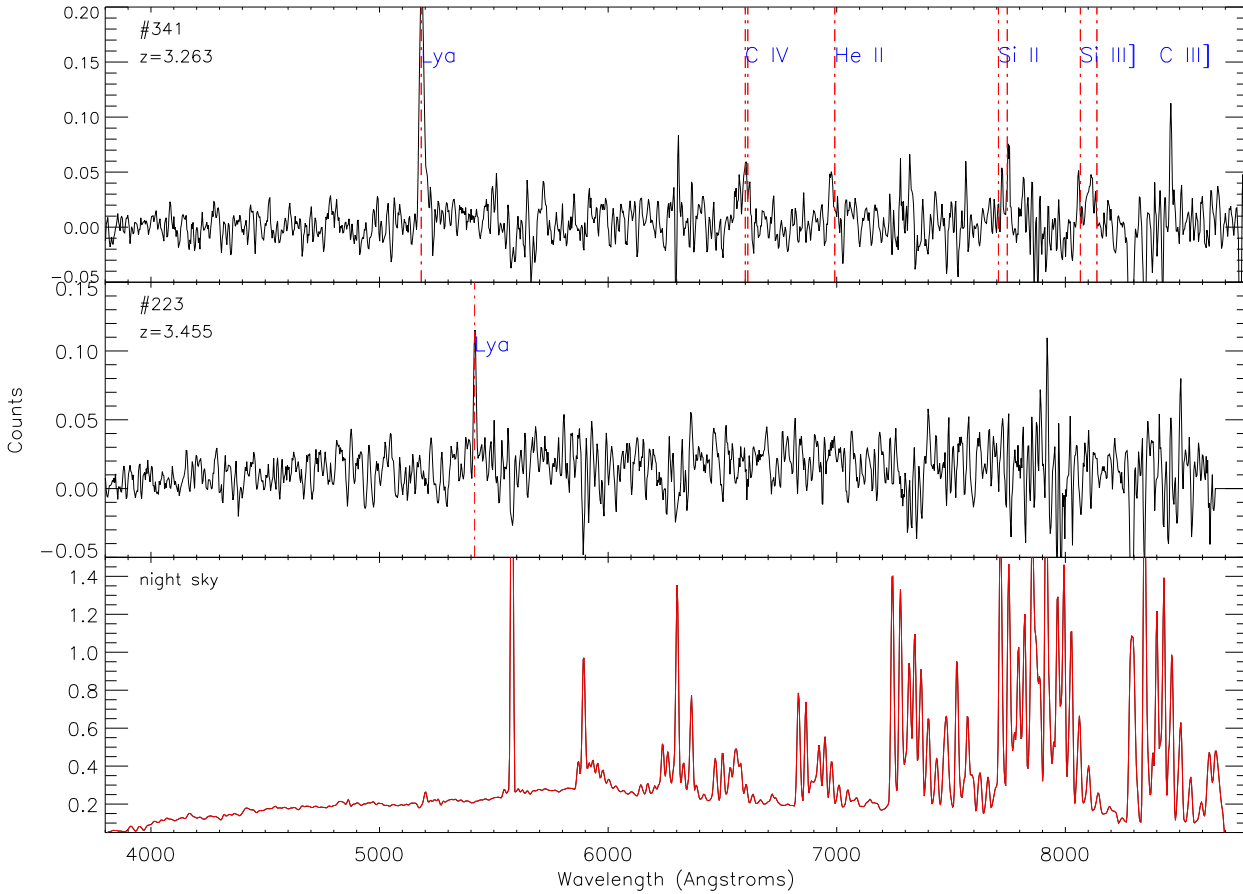


**Fig. 9.** FORS2 spectra of background Ly- $\alpha$  emitters identified in the field of MRC 1138–262.

## 5. Properties of the two confirmed red galaxies in MRC 1138–262

These are the first examples of red galaxies confirmed as members in a proto-cluster above  $z > 2$ . Here we compare their physical properties, insofar as possible with the information available, with the other confirmed proto-cluster members which are generally small, blue, star-forming, Ly- $\alpha$  and H $\alpha$  emitters.

We make use of the multi-wavelength broad-band data to fit spectral energy distributions (SEDs) and deduce ages, masses and star formation rates (SFRs) for these two galaxies. We also calculate the SFRs from the H $\alpha$  line fluxes in the MOIRCS spectra and from *Spitzer* 24  $\mu$ m imaging of the MRC 1138–262 field. Finally, given the projected spatial location with respect to the RG, and the calculated stellar masses, we attempt to infer whether or not these galaxies will eventually merge with MRC 1138–262.

### 5.1. Stellar masses

Using broad-band *UBRIJHK<sub>s</sub>*[3.6][4.5][5.8][8.0] photometry, we fit the SEDs of the two galaxies confirmed to lie at the redshift of the MRC 1138–262 to model templates with two aims. The first is to test if the photometric redshifts produced are reliable, which is useful for future studies. The second is to derive estimates of the physical properties of these galaxies — in particular, their stellar masses. Tanaka et al. (in prep.) describes the

details of the model fitting, but we briefly outline the procedure here.

The model templates were generated using the updated version of Bruzual & Charlot (2003) population synthesis code (Charlot & Bruzual in prep), which takes into account the effects of thermally pulsating AGB stars. We adopt the Salpeter (1955) initial mass function (IMF) and solar and sub-solar metallicities ( $Z = 0.02$  and  $0.008$ ). We generated model templates assuming an exponentially decaying SFR with time scale  $\tau$ , dust extinction, and age. We implement effects of the intergalactic extinction following Furusawa et al. (2000), who used the recipe by Madau (1995), as we are exploring the  $z > 2$  Universe. We use conventional  $\chi^2$  minimizing statistics to fit the models to the observed data.

Firstly, we generate model templates at various redshifts and perform the SED fit. Errors of 0.1 magnitudes are added in quadrature to all bands to ensure that systematic zero point errors do not dominate the overall error budget. The resulting photometric redshift of the object #456 is  $2.25^{+0.06}_{-0.09}$ , which is consistent with the spectroscopic redshift ( $z_{\text{spec}} = 2.1719$ ).

We then fix the redshift of the templates at the spectroscopic redshift and fit the SED again. We impose the logical constraint that the model galaxies must be younger than the age of the Universe. The derived properties of the galaxy #456 are an age of  $1.6^{+1.1}_{-0.7}$  Gyr, an e-folding time scale  $\tau = 0.1^{+0.4}_{-0.1}$  Gyr, and dust extinction of  $\tau_V = 0.4^{+1.4}_{-0.4}$ , where  $\tau_V$  is the optical depth in the V-band. It is a relatively old galaxy with a modest amount of dust,

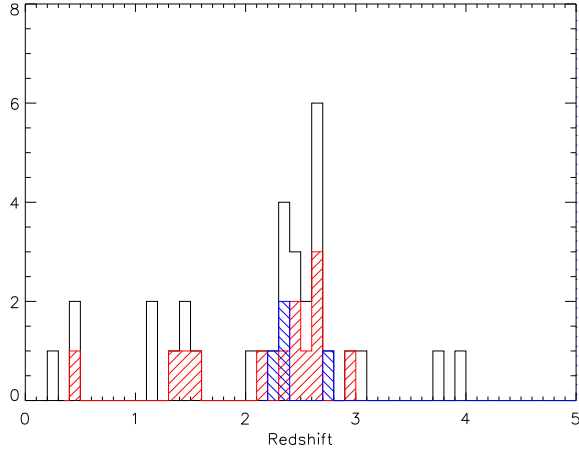


**Fig. 8.** Redshift distribution for confirmed sources in the field of MRC 0943–242 at  $z = 2.93$  (redshift indicated by an arrow). The proportion of sources in each bin with quality flag 1 (i.e. reliable redshifts) is shown with red hatching. The blue hatching shows sources with quality 3 (i.e., representing an upper limit rather than a confirmed redshift). No filling (i.e., simply the black outline) shows all sources with redshifts (quality flags 1 and 2).

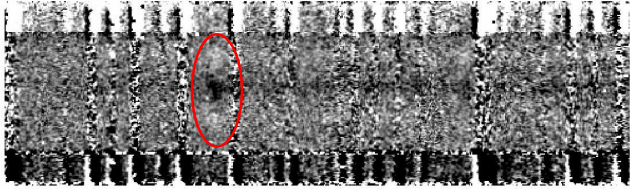
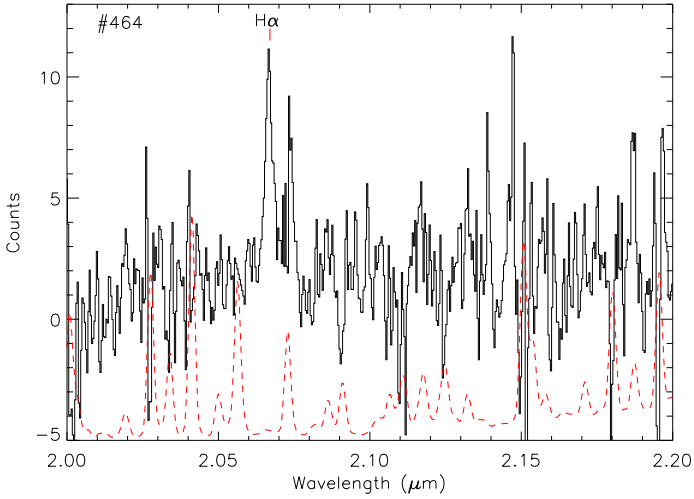


**Fig. 10.** (Bottom) 2D and (top) 1D spectra for the object #464 with  $z=2.149$ . The OH skylines are shown in red underneath the 1D spectrum. The 2D and 1D spectra are on the same wavelength scale.

although the error on the extinction is large. The apparent red color of the galaxy is probably due to its old stellar populations. We find a high photometric stellar mass of  $2.8^{+1.5}_{-1.0} \times 10^{11} M_{\odot}$  for this galaxy. The short time scale derived ( $\tau$  of only 0.1 Gyr) suggests that the galaxy formed in an intense burst of star formation. The low current star formation rate of  $0.0^{+1.0}_{-0.0} M_{\odot} \text{ yr}^{-1}$  derived from the SED fit indeed confirms that the high star for-

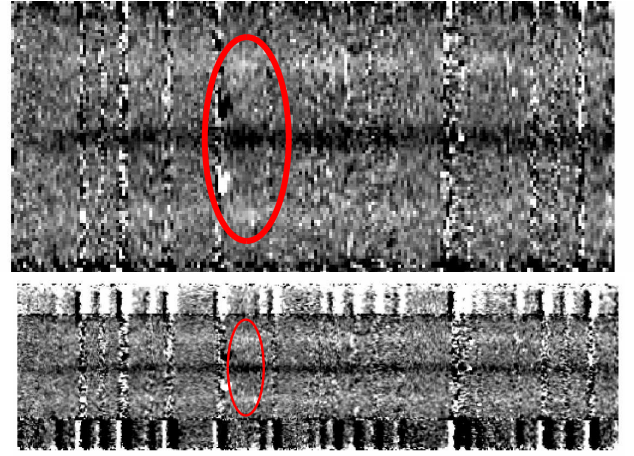
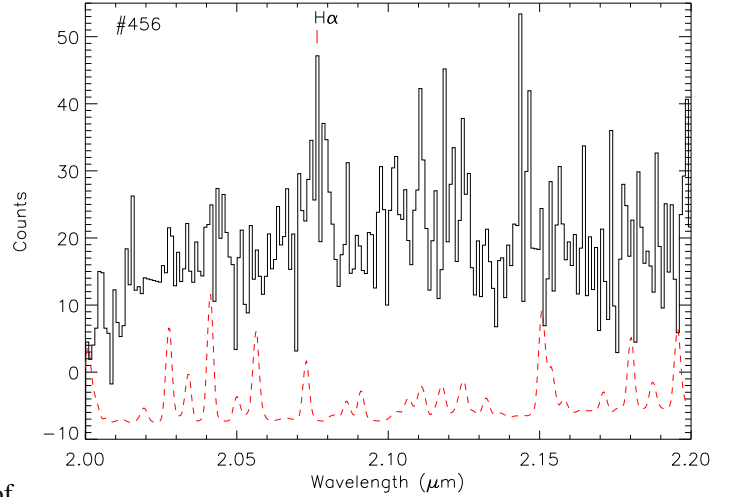


**Fig. 11.** Bottom: 2d spectrum of object #456 showing H- $\alpha$  detection, Middle: 2d spectrum rebinned in 2x2 pixels to emphasize the detection and Top: 1d spectrum extracted from the rebinned 2d spectrum.

mation phase has ended and the galaxy is now in a quiescent phase.

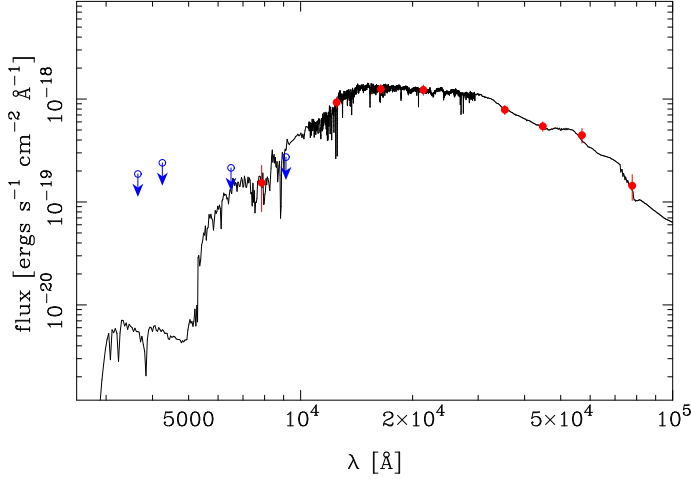
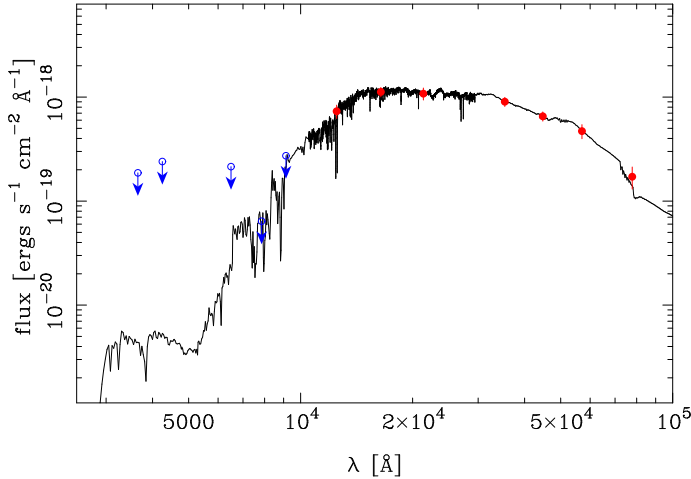
For the galaxy #464, the best fit photometric redshift is  $z_{\text{phot}} = 2.05^{+0.26}_{-0.13}$ , consistent with the spectroscopic redshift ( $z_{\text{spec}} = 2.149$ ). The best fit at the spectroscopic redshift yields an age of  $2.4^{+0.4}_{-1.0}$  Gyr, an e-folding time  $\tau = 0.2^{+0.1}_{-0.2}$  Gyr, dust extinction of  $\tau_V = 0.7^{+0.7}_{-0.6}$ , a stellar mass of  $5.1^{+1.5}_{-2.0} \times 10^{11} M_{\odot}$  and a SFR of  $0.0^{+1.0}_{-0.0} M_{\odot} \text{ yr}^{-1}$ .

The best fitting SEDs for each galaxy are shown in Figures 13 and 12. The broad-band magnitudes of the two galaxies are summarized in Table 5. A more extensive analysis of the properties of galaxies in the MRC 1138–262 field will be presented in Tanaka et al. (in prep.).

Several earlier papers presented measurements of different classes of objects in the field of MRC 1138–262. Kurk et al. (2004b) converted K-band magnitudes to masses, for the Ly- $\alpha$  and H- $\alpha$  emitters, estimating masses of  $0.3 - 3 \times 10^{10} M_{\odot}$  for the Ly- $\alpha$  emitters (except for one object with a mass of  $7.5 \times 10^{10} M_{\odot}$ ) and  $0.3 - 11 \times 10^{10} M_{\odot}$  for the H- $\alpha$  emitters, the latter on average being clearly more massive than the Ly- $\alpha$  emitters. Furthermore Hatch et al. (2009) find stellar masses between  $4 \times 10^8$  and  $3 \times 10^{10}$  for candidate Ly- $\alpha$  emitting companions within 150 kpc of the central RG. Our red galaxies are thus an order of magni-

**Table 5.** Total magnitudes of the two  $H\alpha$  detected galaxies. In this table, the magnitudes are on the AB system for the ease of fitting SEDs. Magnitude limits are  $3\sigma$  limits.

ID	<i>U</i>	<i>B</i>	<i>R</i>	<i>I</i>	<i>Z</i>	<i>J</i>	<i>H</i>	<i>K<sub>S</sub></i>	3.6 $\mu$ m	4.5 $\mu$ m	5.8 $\mu$ m	8.0 $\mu$ m
456	> 26.6	> 26.0	> 25.2	25.15 $\pm$ 0.41	> 24.2	22.19 $\pm$ 0.08	21.27 $\pm$ 0.04	20.72 $\pm$ 0.06	20.11 $\pm$ 0.03	20.00 $\pm$ 0.04	19.69 $\pm$ 0.13	20.24 $\pm$ 0.25
464	> 26.6	> 26.0	> 25.2	> 26.1	> 24.2	22.45 $\pm$ 0.11	21.39 $\pm$ 0.04	20.86 $\pm$ 0.09	19.96 $\pm$ 0.03	19.80 $\pm$ 0.03	19.63 $\pm$ 0.12	20.05 $\pm$ 0.21

**Fig. 12.** SED fit for object #456, with the fainter  $H\alpha$  emission line detection.**Fig. 13.** SED fit for object #464, with the brighter  $H\alpha$  emission line detection.

tude more massive than the most massive Ly- $\alpha$  emitters and 2–3 times more massive than the most massive  $H\alpha$  emitters discovered through NB imaging searches in this field.

### 5.2. Star formation rates

We now use the line fluxes for the two  $H\alpha$  detections to infer a lower limit to the instantaneous SFR. We obtained a rough flux calibration of the spectra by scaling the total flux in the spectrum to the observed  $K_S$  magnitude of the two objects, and assuming a flat spectral throughput in the  $K_S$ -band. As the observed lines are near the centre of the  $K_S$ -band, this approximation does not significantly effect the derived  $H\alpha$  flux, and we assume a calibration uncertainty of  $\approx 20\%$ . Both line detections lie on the edge of weak telluric absorption features be-

tween 20400–20800 Å and also very close to sky lines (especially #458), increasing the measurement uncertainties. The  $H\alpha$  flux of object #464 thus derived is  $1.3 \pm 0.3 \times 10^{-16} \text{ erg s}^{-1} \text{ cm}^{-2}$  and the fainter object, #456, has an  $H\alpha$  flux of  $6.2 \pm 2 \times 10^{-17} \text{ erg s}^{-1} \text{ cm}^{-2}$ . The measured line flux in #464 is fully consistent with the published  $F(H\alpha) = 1.35 \times 10^{-16} \text{ erg s}^{-1} \text{ cm}^{-2}$  derived from narrow-band imaging (Object 229 of Kurk et al. 2004b). The previously published near-IR spectroscopy of Kurk et al. (2004a) found  $F(H\alpha) = 7.1 \pm 1.9 \times 10^{-17} \text{ erg s}^{-1} \text{ cm}^{-2}$ , which is somewhat lower than our flux, suggesting possible slit losses. In the same narrow-band image, object #458 does not show any excess flux compared to the full  $K$ -band image, suggesting that our line flux may be overestimated due to incomplete skyline subtraction.

Using the Kennicutt (1998) relation,

$$\text{SFR} (M_{\odot} \text{ yr}^{-1}) = 7.9 \times 10^{-42} L(H\alpha) \text{ erg s}^{-1},$$

which assumes solar metallicities and a Salpeter (1955) IMF, this leads to SFRs of  $35 \pm 8$  and  $17 \pm 6 M_{\odot} \text{ yr}^{-1}$ , respectively.

The SFRs derived from  $H\alpha$  are higher than those from the SED fits (Figs 12 and 13), which give SFR up to  $4 M_{\odot} \text{ yr}^{-1}$  at  $2\sigma$ , i.e. a factor of 5–10 lower. An additional independent estimate for the SFR can be obtained from the MIPS 24 $\mu$ m imaging of the field (Seymour et al. 2007). Object #464 is detected at  $S(24\mu\text{m}) = 470 \pm 30 \mu\text{Jy}$ , while object #458 remains undetected at the  $2\sigma < 60 \mu\text{Jy}$  level. We first convert the 24 $\mu$ m flux to the total IR flux using the relation of Reddy et al. (2006), and converted the latter to a SFR using the formula of Kennicutt (1998). The derived SFR are 34 and  $< 4 M_{\odot} \text{ yr}^{-1}$  for objects #464 and #458, respectively. For #464, this is fully consistent with the SFR derived from  $H\alpha$ , but for #458, the value derived from  $H\alpha$  seems strongly over-estimated. This may be either be due to the low S/N and incomplete skyline removal in our near-IR spectroscopy, or it may indicate that the  $H\alpha$  may have a contribution by an AGN. To confirm the latter hypothesis, we need to obtain other emission lines such [OIII], but the possible AGN contribution may not be surprising given the higher fraction of AGNs observed in proto-clusters (e.g. Galametz et al. 2009).

In summary, we find that object #458 most likely belongs to the class of passively evolving galaxies, while #464 belongs to the class of dusty star-forming red galaxies.

### 5.3. Merging timescales

The spatial locations of the two red galaxies identified at the redshift of MRC 1138–262 are shown in Figure 14. They both lie along the East-West axis, where most of the confirmed AGN in this field were found (Croft et al. 2005; Pentericci et al. 2002) and where the brighter DRGs in Kodama et al. (2007) also trace a filament. The two galaxies are relatively central, being located within  $1'$  (500 kpc, physical) of the radio galaxy. This is significant given that no obvious density gradient has been observed for the Lyman- $\alpha$  emitters (e.g., Pentericci et al. 2000; Kurk et al. 2003), yet Kurk et al. (2004b) argue there is an indication that

the  $H\alpha$  emitters and extremely red objects have a higher density near the RG than further out. Our new results and these former results are consistent with the picture that accelerated evolution takes place in high density environments.

To properly assess the possibility of a future merger between the RG and one or both of the red companion galaxies, numerical simulations are needed. However, we can at least gain an idea of the relative timescales involved as follows. The crossing time can be approximated by  $t_{\text{cross}} = (R^3/GM_{\text{total}})^{1/2}$  (Binney & Tremaine 2008) where  $R$  is the distance between the two galaxies and  $M$  is the total mass (dark matter + stellar) of the central galaxy, approximately  $10^{13}M_{\odot}$  in this case (Hatch et al. 2009). For the closer galaxy to the RG, #464, the distance is  $R \sim 300$  kpc (physical) and the crossing time is therefore roughly 0.7 Gyr. The second galaxy has a crossing time between 2–3 times longer, let us say approximately 2 Gyr. For a major merger (unless it is a high speed encounter in which case the galaxies would pass through each other with little disruption) the galaxies should merge into a single system within a few crossing times (Binney & Tremaine 2008). There is therefore enough time for the two red galaxies to merge with the central RG before redshift  $z = 0$ , increasing its stellar mass of  $10^{12}M_{\odot}$  (Hatch et al. 2009) by a factor of at least 50%.

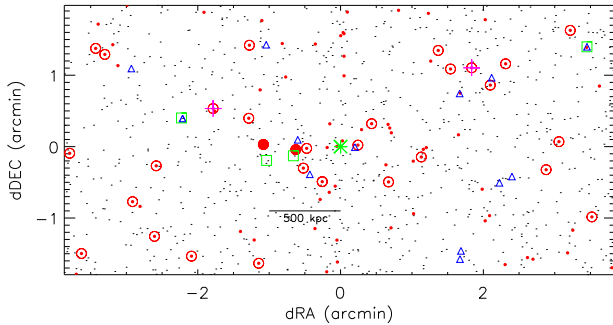


**Fig. 14.** Relative spatial distribution of the two confirmed massive galaxies in MRC 1138–262. The central radio galaxy is marked by a large green asterisk. The red galaxy candidates are marked as red points; those targeted spectroscopically are marked with circles. The two filled red circles are the galaxies confirmed to lie at the redshift of the radio galaxy. Confirmed Lyman- $\alpha$  emitters are marked as blue triangles (Pentericci et al. 2000), and confirmed AGN are marked as the smaller green squares (Croft et al. 2005; Pentericci et al. 2002). Objects which have been excluded as background objects are marked with a plus sign.

## 6. Conclusions

We observed a total of 57 near-infrared selected galaxies in MRC 0943–242 and 33 in MRC 1138–262 with a mix of optical and near-infrared multi-object spectroscopy to attempt the confirmation of massive galaxies in the vicinity of the central radio galaxy in these candidate forming proto-clusters. We have determined that the  $JHK_s$  selection criteria presented in

Kajisawa et al. (2006) select mostly  $2.3 < z < 3.1$  galaxies, thus confirming the validity of this colour selection technique (10 out of 18 confirmed redshifts of  $JHK_s$ -selected galaxies are in this redshift range). Of the 57 sources in the field of the radio galaxy MRC 0943–242 we identify 27 spectroscopic redshifts and for the remaining 30 sources we obtained five upper limits on the redshifts, excluding them to be part of the proto-cluster. The remaining 25 objects could not be excluded as either foreground or background. An unknown fraction of these may be at the redshift of the radio galaxy. However, we also pinpoint a foreground (but still quite distant) large scale structure at redshift  $z \approx 2.65$  in this field, so it is likely that some of the remaining galaxies are also associated with this structure.

Of the 33 galaxies observed in MRC 1138–262 we exclude two background objects and confirm two objects at the redshift of the radio galaxy (all on the basis of emission lines). We cannot exclude the remaining 29 objects as being potential proto-cluster members — we require deep near-infrared spectroscopy to locate the 4000Å break. On the basis of SED fits, and the SFR derived from both the  $H\alpha$  line flux and the 24  $\mu\text{m}$  flux, we deduce that one of the two red galaxies confirmed to be at the redshift of the proto-cluster belongs to the class of dusty star-forming (but still massive) red galaxies, while the other is evolved and massive, and formed rapidly in intense bursts of star formation. This represents the first red galaxies to be confirmed as a member of a proto-cluster above  $z > 2$ . The only other galaxies of the same class are evolved galaxies found in an overdensity at  $z = 1.6$  in the Galaxy Mass Assembly ultra-deep Spectroscopic Survey (Kurk et al. 2009), and red massive galaxies in the Multi-wavelength Survey by Yale-Chile (MUSYC) sample at  $z \sim 2.3$  (e.g. Kriek et al. 2006). Since their phase of high star formation has ended (the current SFR is of order  $1 M_{\odot} \text{ yr}^{-1}$ ), we only just detect them through their emission line fluxes. However, this shows that even in these galaxies where we do not expect strong emission lines, it is still sometimes possible to derive redshifts from the  $H\alpha$  line. It is highly likely that there are more galaxies on the red sequence in this field which have completely ceased star formation and are thus very difficult to identify spectroscopically. The next stage of our spectroscopic campaign is to obtain deep near-infrared spectroscopy in the  $J$ - and  $H$ -bands to search for objects with 4000Å continuum breaks.

Given the inferred SFRs and stellar masses of the two confirmed  $z \sim 2.15$  galaxies, they have to have formed quite early, which fits into the down-sizing scenario (Cowie et al. 1996). Although this conclusion is drawn from limited numbers, the low fraction of sources with  $H\alpha$  emission lines in our sample suggests that most of the sources probably don't have much on-going star formation ( $\text{SFR} < 0.5 M_{\odot} \text{ yr}^{-1}$ ) and so their formation epoch might be quite high. This would be contrary to the idea of the giant elliptical assembly epoch being  $z \sim 2 - 3$  (e.g., van Dokkum et al. 2008; Kriek et al. 2008), but is consistent with results from SED age fitting of stellar populations, which point to  $z_{\text{form}} > 3$  (e.g., Eisenhardt et al. 2008). The discrepancy may be resolved if subclumps form early and merge without inducing much star formation (i.e. dry merging). Alternatively, the fact that these galaxies are located in over-densities may predispose us to structures that formed early.

Finally, the proximity of these two massive galaxies to the RG implies that they will have an important impact on its future evolution. Given the crossing times, compared with the time remaining until  $z = 0$ , it is plausible that one or both of the galaxies may eventually merge with the RG.

**Acknowledgements.** We thank the referee G. Zamorani for a very constructive referee report, which has substantially improved this paper. This work was financially supported in part by the Grant-in-Aid for Scientific Research (No.s 18684004 and 21340045) by the Japanese Ministry of Education, Culture, Sports and Science. CL is supported by NASA grant NNX08AW14H through their Graduate Student Researcher Program (GSRP). We thank Dr. Bruzual and Dr. Charlot for kindly providing us with their latest population synthesis code. MD thanks Andy Bunker and Rob Sharp for useful discussions on manipulating MOIRCS data. The work of DS was carried out at Jet Propulsion Laboratory, California Institute of Technology, under a contract with NASA. JK acknowledges financial support from DFG grant SFB 439. The authors wish to respectfully acknowledge the significant cultural role and reverence that the summit of Mauna Kea has always had within the indigenous Hawaiian community. We are fortunate to have the opportunity to conduct scientific observations from this mountain.

## References

- Appenzeller, I. & Rupprecht, G. 1992, *The Messenger*, 67, 18
- Binney, J. & Tremaine, S. 2008, *Galactic Dynamics: Second Edition* (Princeton University Press)
- Blakeslee, J. P., Franx, M., Postman, M., et al. 2003, *ApJ*, 596, L143
- Bruzual, G. & Charlot, S. 2003, *MNRAS*, 344, 1000
- Cowie, L. L., Songaila, A., Hu, E. M., & Cohen, J. G. 1996, *AJ*, 112, 839
- Croft, S., Kurk, J., van Breugel, W., et al. 2005, *AJ*, 130, 867
- D’Odorico, S., Dekker, H., Mazzoleni, R., et al. 2006, in *Society of Photo-Optical Instrumentation Engineers (SPIE) Conference Series*, Vol. 6269, Society of Photo-Optical Instrumentation Engineers (SPIE) Conference Series
- Eisenhardt, P. R. M., Brodwin, M., Gonzalez, A. H., et al. 2008, *ApJ*, 684, 905
- Eke, V. R., Cole, S., & Frenk, C. S. 1996, *MNRAS*, 282, 263
- Ellis, S. C., Jones, L. R., Donovan, D., Ebeling, H., & Khosroshahi, H. G. 2006, *MNRAS*, 368, 769
- Förster Schreiber, N. M., van Dokkum, P. G., Franx, M., et al. 2004, *ApJ*, 616, 40
- Furusawa, H., Shimasaku, K., Doi, M., & Okamura, S. 2000, *ApJ*, 534, 624
- Galametz, A., Stern, D., Eisenhardt, P. R. M., et al. 2009, *ApJ*, 694, 1309
- Goldoni, P., Royer, F., François, P., et al. 2006, in *Society of Photo-Optical Instrumentation Engineers (SPIE) Conference Series*, Vol. 6269, Society of Photo-Optical Instrumentation Engineers (SPIE) Conference Series
- Grazian, A., Fontana, A., Moscardini, L., et al. 2006, *A&A*, 453, 507
- Grazian, A., Salimbeni, S., Pentericci, L., et al. 2007, *A&A*, 465, 393
- Hatch, N. A., Overzier, R. A., Kurk, J. D., et al. 2009, *MNRAS*, 395, 114
- Hilton, M., Collins, C. A., Stanford, S. A., et al. 2007, *ApJ*, 670, 1000
- Ichikawa, T., Suzuki, R., Tokoku, C., et al. 2006, in *Presented at the Society of Photo-Optical Instrumentation Engineers (SPIE) Conference*, Vol. 6269, Society of Photo-Optical Instrumentation Engineers (SPIE) Conference Series
- Kajisawa, M., Kodama, T., Tanaka, I., Yamada, T., & Bower, R. 2006, *MNRAS*, 371, 577
- Kashikawa, N., Inata, M., Iye, M., et al. 2000, in *Society of Photo-Optical Instrumentation Engineers (SPIE) Conference Series*, Vol. 4008, Society of Photo-Optical Instrumentation Engineers (SPIE) Conference Series, ed. M. Iye & A. F. Moorwood, 104–113
- Kennicutt, R. C. 1998, *ARA&A*, 36, 189
- Kodama, T., Bell, E. F., & Bower, R. G. 1999, *MNRAS*, 302, 152
- Kodama, T., Tanaka, I., Kajisawa, M., et al. 2007, *MNRAS*, 377, 1717
- Kriek, M., van der Wel, A., van Dokkum, P. G., Franx, M., & Illingworth, G. D. 2008, *ApJ*, 682, 896
- Kriek, M., van Dokkum, P. G., Franx, M., et al. 2006, *ApJ*, 645, 44
- Kurk, J., Cimatti, A., Zamorani, G., et al. 2009, *ArXiv e-prints*
- Kurk, J., Röttgering, H., Pentericci, L., Miley, G., & Overzier, R. 2003, *New Astronomy Review*, 47, 339
- Kurk, J. D., Pentericci, L., Overzier, R. A., Röttgering, H. J. A., & Miley, G. K. 2004a, *A&A*, 428, 817
- Kurk, J. D., Pentericci, L., Röttgering, H. J. A., & Miley, G. K. 2004b, *A&A*, 428, 793
- Lidman, C., Rosati, P., Tanaka, M., et al. 2008, *A&A*, 489, 981
- Madau, P. 1995, *ApJ*, 441, 18
- Pentericci, L., Kurk, J. D., Carilli, C. L., et al. 2002, *A&A*, 396, 109
- Pentericci, L., Kurk, J. D., Röttgering, H. J. A., et al. 2000, *A&A*, 361, L25
- Reddy, N. A., Steidel, C. C., Fadda, D., et al. 2006, *ApJ*, 644, 792
- Rieke, G. H., Young, E. T., Engelbracht, C. W., et al. 2004, *ApJS*, 154, 25
- Salpeter, E. E. 1955, *ApJ*, 121, 161
- Seymour, N., Stern, D., De Breuck, C., et al. 2007, *ApJS*, 171, 353
- Spergel, D. N., Verde, L., Peiris, H. V., et al. 2003, *ApJS*, 148, 175
- Stanford, S. A., Romer, A. K., Sabirli, K., et al. 2006, *ApJ*, 646, L13
- Suzuki, R., Tokoku, C., Ichikawa, T., et al. 2008, *PASJ*, 60, 1347
- Tanaka, M., Kodama, T., Arimoto, N., et al. 2005, *MNRAS*, 362, 268
- van Dokkum, P. G., Franx, M., Förster Schreiber, N. M., et al. 2004, *ApJ*, 611, 703
- van Dokkum, P. G., Franx, M., Kriek, M., et al. 2008, *ApJ*, 677, L5
- van Dokkum, P. G. & Stanford, S. A. 2003, *ApJ*, 585, 78
- van Dokkum, P. G., Stanford, S. A., Holden, B. P., et al. 2001, *ApJ*, 552, L101
- Venemans, B. P., Röttgering, H. J. A., Miley, G. K., et al. 2005, *A&A*, 431, 793
- Venemans, B. P., Röttgering, H. J. A., Miley, G. K., et al. 2007, *A&A*, 461, 823
- Zirm, A. W., Stanford, S. A., Postman, M., et al. 2008, *ApJ*, 680, 224